Differences in the mirror reactions $^3H(p,\gamma)^4He$ and $^3He(n,\gamma)^4He$ from an isospin conserving nuclear force

B. Wachter, T. Mertelmeier, and H. M. Hofmann
Institute for Theoretical Physics, University of Erlangen-Nürnberg, D-8520 Erlangen, Federal Republic of Germany
(Received 11 May 1988)

The radiative capture reactions $^3H(p,\gamma)^4He$ and $^3He(n,\gamma)^4He$ are studied within the framework of a microscopic multichannel resonating group model. Employing a charge symmetric nuclear force we find different thresholds for the mirror channels due to the Coulomb force. These differences in term together with channel coupling effects lead to marked variations between observables of the two mirror reactions. We demonstrate that all types of experimental data can be reproduced by our calculation except for the controversial integrated (n,γ) cross section data.

I. INTRODUCTION

In recent years the strict validity of the general symmetry laws in the strong nuclear interaction became more and more questionable. In particular, it has been suggested that charge independence of nuclear forces is violated. This symmetry violation can be explored in a number of different ways. Especially comparison of mirror reactions have been used to investigate the existence of charge symmetry violation of nuclear forces. Naively the differential cross sections and polarization observables of the mirror reactions are expected to be identical. The Coulomb interaction, however, breaks charge symmetry, hence, conclusions from such experiments may not be straightforwardly drawn. In very light nuclei, Coulomb effects are expected to be small and therefore few body reactions are favorable processes.

In the mirror reactions $^2H(d,p)^3H$ and $^2H(d,n)^3He$ only small charge symmetry violations were found[1] after Coulomb effects have been approximately taken into account.

On the other hand, photonuclear reactions offer the possibility of extracting a small but nonzero charge asymmetry because of the extreme sensitivity of the cross section to the degree of isospin mixing.[2] Especially in the mirror reactions $^4He(\gamma,p)^3H$ and $^4He(\gamma,n)^3He$ large differences in the total cross section were reported in the giant dipole resonance region.[3,4] This is in marked disagreement with model calculations,[5] therefore charge symmetry breaking nuclear forces were introduced in order to reproduce the data.[6]

In the following we report on a microscopic calculation in the framework of the resonating group method which takes into account Coulomb effects exactly; especially the different thresholds for the mirror channels are correctly reproduced.

The calculation of the radiative capture reactions to ^4He is based on a detailed study of the ^4He system.[7] Results on the $^2He(d,\gamma)^4He$ reaction with emphasis on the D-state admixture in the ^4He ground state were reported elsewhere.[8,9] Here we concentrate on the reactions $^4He(\gamma,p)^3H$ and $^4He(\gamma,n)^3He$. For the convenience of the reader we first give an overview on the method used. After that we present results on differential cross sections and polarizations and discuss the differences in both reactions.

II. METHOD

Because of the weakness of the electromagnetic interaction radiative processes can be treated in Born approximation. A process like $^3H(p,\gamma)^4He$ presupposes the knowledge of the wave function of the ^4He ground state as well as a solution of the ^3H+p scattering problem. The wave function in the interaction region of the fragments contributes to the radiative process, hence, proper antisymmetrization of the nucleons has to be taken into account, whereby the identity of the incoming particles is destroyed. Therefore, the coupling to other channels has to be treated consistently. In our case the strong channels consist of ^3H+p, ^3He+n, and ^2H+d. The resonating group model is well suited to treat such multichannel problems on the basis of a microscopic nucleon-nucleon interaction. Furthermore, translational invariance which is vital in light systems, is automatically guaranteed.

Starting from a semirealistic nucleon-nucleon force,[10] which contains besides the Coulomb force central, spin-orbit, and tensor components, we determined the scattering wave functions as consisting of ^3H+p, ^3He+n, and $d+d$ components from the variational principle

$$\langle \delta\psi \mid H-E \mid \psi \rangle = 0 \ . \tag{1}$$

This part of the calculation parallels the work reported earlier.[7] All the internal wave functions are S states only, the parameters are given in Ref. 7, and all the scattering results, like phase shifts, etc., are identical to those found previously.[7] Angular momenta up to $L=2$ are allowed in the relative motion of the fragments, because all other phase shifts and corresponding matrix elements are small. A detailed description of the method can be found in Refs. 11 and 12.

The wave function of the ^{4}He ground state is determined by searching for the most strongly bound 0^+ state in the above function space. Since no internal orbital angular momenta are taken into account, the 0^+ ground-state wave function is a linear combination of the following form (for the notation see Ref. 12).

$$\begin{aligned}\psi^{0+}=\mathcal{A}\{&[(\phi^{^3\mathrm{H}}\phi^{p})^{S_c=0}Y_0(\hat{\mathbf{R}}_{^3\mathrm{H}p})R_{^3\mathrm{H}p}^{-1}]^{0+}\chi^0_{^3\mathrm{H}p}(R_{^3\mathrm{H}p})\\&+[(\phi^{^3\mathrm{He}}\phi^{n})^{S_c=0}Y_0(\hat{\mathbf{R}}_{^3\mathrm{He}n})R_{^3\mathrm{He}n}^{-1}]^{0+}\chi^0_{^3\mathrm{He}n}(R_{^3\mathrm{He}n})\\&+[(\phi^{d}\phi^{d})^{S_c=0}Y_0(\hat{\mathbf{R}}_{dd})R_{dd}^{-1}]^{0+}\chi^0_{dd}(R_{dd})+[(\phi^{d}\phi^{d})^{S_c=2}Y_2(\hat{\mathbf{R}}_{dd})R_{dd}^{-1}]^{0+}\chi^2_{dd}(R_{dd})\}\ .\end{aligned}\tag{2}$$

In obvious notation the spins of the fragments are coupled to the channel spin S_c which is then coupled with the relative orbital angular momentum L to the total angular momentum J. The relative motion wave functions χ^L depend on the radial distance R between the fragments indicated.

In case of a bound state calculation the χ^L are linear superpositions of Gaussian functions in the form

$$\chi^L_{\mathrm{bound}}(R)=R^{L+1}\sum_{i=1}^{N}\alpha_i\exp(-\beta_i R^2)\ .\tag{3}$$

The width parameters β_i and the coefficients α_i are determined by a minimization routine. For each component of the wave function, Eq. (2), three Gaussian functions for the relative motion approximated well the ground state. Since, for small energies, the radiative capture takes place in the asymptotic region of the wave function we added another Gaussian function with an appropriate width parameter in order to reproduce the tail of the Whittaker functions corresponding to the experimental separation energies. In the radiative capture of ^{3}He on ^{4}He it was shown[10] that this procedure yields reliable results down to about 50 keV.

In a scattering calculation the asymptotic form of the wave function is accounted for by the ansatz

$$\begin{aligned}\chi^L_{lk\ \mathrm{scatt}}(R_k)=&\delta_{lk}F^L(R_k)+a_{lk}G^L(R_k)\\&+\Sigma_m b_{lkm}R_k^{L+1}\exp(-\beta_m R_k^2)\ ,\end{aligned}\tag{4}$$

where F_L and G_L are regular and irregular Coulomb functions and the Gaussians take distortions in the nuclear interaction region into account. The index k runs over all possible channels and the index l indicates the boundary condition, namely in which channel there are regular waves. In the scattering calculation the expansion coefficients b_{lkm} and the elements of the reactance matrix a_{lk} are linear variational parameters.

Since the physical process consists of incoming waves in one particular channel and outgoing waves in all the others, we have to proceed from the real scattering wave function, Eq. (4), corresponding to standing waves, to complex wave functions by multiplying the whole set χ^L_{lk} with the matrix

$$C_{jl}=[(1-ia)^{-1}]_{jl}\ ,\tag{5}$$

where a is again the reactance matrix of Eq. (4). Details of the angular momentum coupling and phases are given elsewhere.[10] In passing we note that applying C results in additional coupling of the channels and leads to complex matrix elements [see Eq. (8)].

The calculation of the radiative capture matrix elements was performed as in Ref. 10. The electromagnetic transition operators (electric orbital, electric spin, magnetic orbital, and magnetic spin) are taken in the long wavelength limit. The electric orbital operator stems from Siegert's theorem,[13] hence, it includes the main part of the meson exchange currents, whereas the other operators do not.[14] Charges and g factors for free nucleons are used.

The normalization and phase conventions of Seyler and Weller were adopted.[15] Since our scattering wave function contains p-^{3}H, n-^{3}He, and d-^{2}H components simultaneously, we can calculate the reactions ^{2}H$(d,\gamma)^4$He, ^{3}H$(p,\gamma)^4$He, and ^{3}He$(n,\gamma)^4$He by just varying the boundary condition. Here we report on results of the ^{3}H$(p,\gamma)^4$He and ^{3}He$(n,\gamma)^4$He reactions, the deuteron capture was discussed elsewhere.[8,9]

III. RESULTS

The main interest in the mirror reactions ^{3}H$(p,\gamma)^4$He and ^{3}He$(n,\gamma)^4$He lies in the different magnitudes of the integrated cross section.[3,4] Therefore, we study in the following the leading transition matrix elements for both reactions. We characterize them by the incoming channels denoted by $^{2S+1}L_J$, where $\mathbf{S}+\mathbf{L}=\mathbf{J}$.

In Fig. 1 we display the moduli of the largest matrix elements for all three fusion reactions. Matrix elements not displayed are still smaller and furthermore they do not interfere with the leading one, hence, they lead only to minor corrections of the observables. As anticipated, the $^1P_1-E1$ matrix elements are the largest ones in both reactions studied here, whereas the suppression of the deuteron-deuteron capture becomes obvious. Therefore, we need not consider the influence of this reaction further on. Figure 1 shows that the leading ^{3}H$+p$ matrix element is somewhat larger than the corresponding ^{3}He$+n$ matrix element.

In the following we analyze this difference in detail. Classically, the electric dipole moment for ^{3}H$+p$ has the same magnitude as the ^{3}He$+n$ dipole moment but the opposite sign for analogous configurations. Therefore, we anticipate the orbital matrix elements to be of equal size

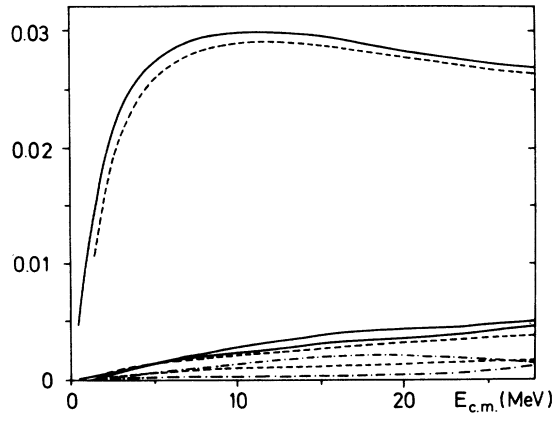

FIG. 1. The moduli of the largest radiative capture matrix elements are shown as function of the center-of-mass energy above the ^3H+p threshold for the reactions $^3H(p,\gamma)^4He$ (full lines). $^3He(n,\gamma)^4He$ (dashed lines), and $^2H(d,\gamma)^4He$ (dot-dashed lines). For the first two reactions the matrix elements occur in the order $^1P_1-E1 > {}^3P_1-E1 > {}^1D_2-E2$ and for the $^2H(d,\gamma)^4He$ reaction $^1D_2-E2 > {}^3P_1-E1$.

but opposite sign, too. The spin-flip matrix element, which is supposed to be small, originates solely from the coupling to the $^3P_1$ channels in the interaction region. The dominant part of this comes from the single nucleon. Since the relation of the nuclear magnetic moment is $g_p=-1.46g_n$, the difference of the total matrix elements should be less than a third of the proton spin matrix elements.

Depending on the energy, however, the size of the spin matrix element is only a few percent of the orbital matrix element, leading to differences much smaller than those displayed in Fig. 1. A detailed analysis of the matrix elements reveals that the differences found are due to differences in the orbital matrix element.

Whereas the classical argument given above presupposes equal distances between the two fragments in both cases, our calculated scattering wave functions exhibit small differences between the ^3He+p and ^3He+n channels. This is due to the different kinetic energy in both channels because of the different binding energy originating from the Coulomb force. If we consider orbital matrix elements corresponding to equal kinetic energy in both channels, we find no difference after eliminating effects of the γ energy. Therefore, we conclude that the differences found are solely due to the Coulomb force.

Returning to Fig. 1 we find one matrix element dominating all the others by more than one order of magnitude. Therefore, the differential cross section will depend mainly on this matrix element and only those matrix elements interfering with the leading one have to be considered. The differential cross section can be expanded in terms of Legendre polynomials

$$\frac{d\sigma}{d\Omega}(\vartheta)=A_0\left[1+\sum_{n=1}A_nP_n(\cos\vartheta)\right] . \tag{6}$$

The coefficients A_0 and $A_0\cdot A_n$ are given as bilinear combinations of the contributing matrix elements by some Racah algebra. Restricting to multipolarities 1 and 2, the $^1P_1-E1$ matrix element can only contribute to the coefficients A_0 through A_3. In A_0 and $A_0\cdot A_2$ it contributes quadratically with a coefficient of equal size but opposite sign. Because of the normalization in Eq. (6), A_2 has to be -1 as long as interference terms can be neglected. This holds true up to 10 MeV kinetic energy (see Fig. 2) for higher energies deviations from -1 of about 15% occur.

In A_1 and A_3 the $E1$ matrix element interferes solely with the next larger matrix element $^1D_2-E2$, again with coefficients of equal size and opposite sign. Thus A_1 should be $-A_3$, as can be seen in Fig. 2. Note that the relevant coefficient in A_1 is about three times the coefficient in A_0. As expected, the coefficient A_4 is small compared to all the others, therefore we do not show it for the ^3He+n case.

But there is a striking difference in the A_1 and A_3 coefficient for the ^3He+n case and the ^3H+p case. This is similar to the results of a shell model calculation.[5] As discussed above, these coefficients are due to the interference of the $^1P_1-E1$ and the $^1D_2-E2$ matrix elements. Since the magnitudes of these matrix elements differ only slightly for the two reactions (see Fig. 1), the variations of the coefficients A_1 and A_3 originate from the phases involved, occurring in the form

$$\cos[\delta(^1P_1)-\delta(^1D_2)] , \tag{7}$$

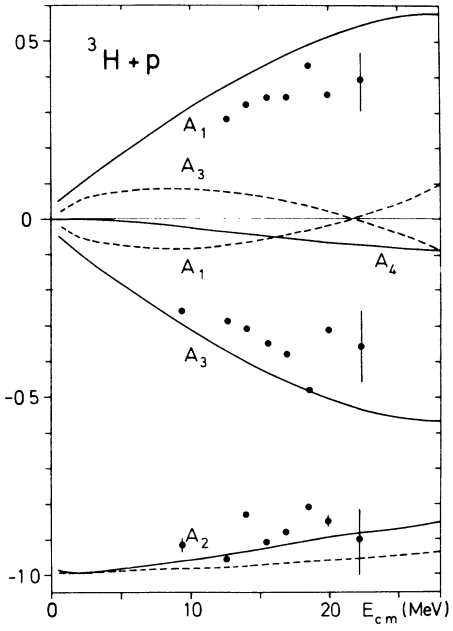

FIG. 2. Calculated Legendre expansion coefficients of the differential cross section, Eq. (6), are compared with data (Ref. 16) for the $^3H(p,\gamma)^4He$ reaction (full lines). To emphasize the variations between the two mirror channels we also display the calculated results for the $^3He(n,\gamma)^4He$ reaction (dashed lines), but omit the data (Ref. 17) because of their large errors. Note the different signs for A_1 and A_3 for the two mirror reactions at low energy.

where the transition matrix element is written as $S = |S| \cdot \exp\{i\delta\}$. In Fig. 3 we display the relevant phases. Both $^1P_1$ phases show little energy dependence and so does the $^1D_2$ ^{3}H+p phase. The ^{3}He+n $^1D_2$ phase, however, decreases rapidly with energy, thus causing a sign change of the cosine in Eq. (7).

Whereas a classical consideration of both two-body systems reveals equal size for both dipole moments the same consideration yields a quadrupol moment for the ^{3}H+p system five times larger than that of ^{3}He+n. For the $E1$ transitions this classical argument fully agrees with the results found, whereas for the $E2$ matrix element the variations are below a factor 2 (see Fig. 1). Therefore we have to analyze the contributions of the individual channels (we will call this "immediate" contributions) in contrast to the asymptotic mixing due to Eq. (5).

In fact, the immediate contribution of the ^{3}H+p channel is a factor 3–4 larger than that of the ^{3}He+n channel, almost independent of energy. Although in principle all seven $J^\pi = 2^+$ channels are coupled, the strongest part of the nuclear force conserves the spin, therefore the matrix C, Eq. (5), connects dominantly the $^1D_2$ channels and we can concentrate our considerations onto these channels. The magnitude of these reactance matrix elements is nearly the same for all channels except near and obviously below thresholds. Since the immediate contribution to the $^1D_2$ dd channel never exceeds 10% of the leading one, we are left with a two channel problem. The

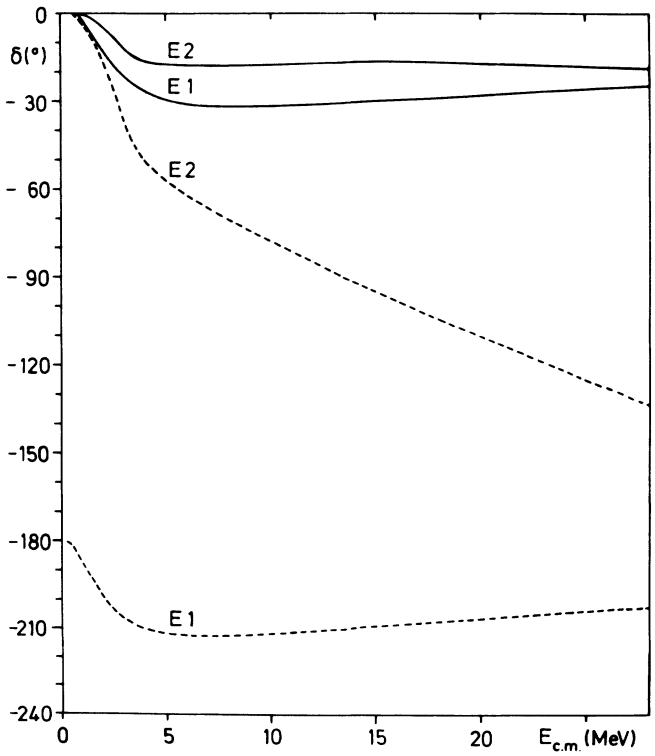

FIG. 3. The phases of the interfering $E1$ and $E2$ matrix elements are given as function of the center-of-mass energy above the lowest threshold for the reactions ^{3}H$(p,\gamma)^4$He (full lines) and ^{3}He$(n,\gamma)^4$He (dashed lines).

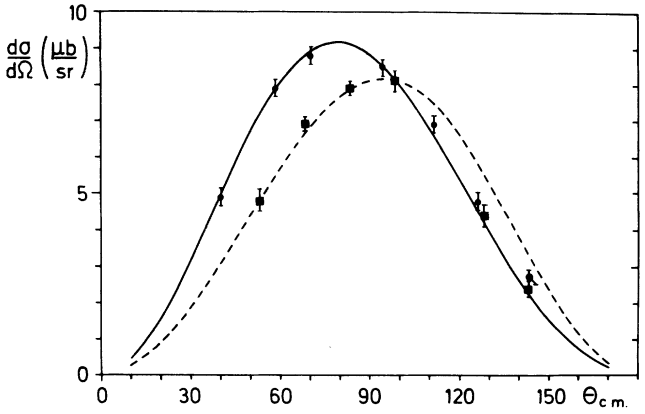

FIG. 4. Comparison of calculated angular distribution for the reactions ^{3}H$(p,\gamma)^4$He (full line) at 9.8 MeV proton energy with data Ref. 18 (full circles) and of the reaction ^{3}He$(n,\gamma)^4$He (dashed line) at 10 MeV neutron energy with data Ref. 17 (open squares). The unnormalized data are normalized to the calculated results at the data point nearest to 90°.

corresponding reactance matrix elements vary from $a = 0.1$ at low energies to about $a = 0.5$ at higher energies. Let us normalize the immediate contribution of the $^1D_2$ ^{3}H+p channel to 1, then the ^{3}He+n channel contributes by $b \approx 0.3$. Applying Eq. (5), schematically for small a, we find for the final matrix elements

$$\begin{bmatrix} 1-ia & -ia \\ -ia & 1-ia \end{bmatrix}^{-1} \begin{bmatrix} 1 \\ b \end{bmatrix} \approx \begin{bmatrix} 1+ia \\ b+ia \end{bmatrix} . \tag{8}$$

The resulting matrix element for the ^{3}H+p channel is of order 1 and the energy dependence is in the small part ia. This explains the small phase of the resultant ^{3}H+p matrix element throughout the energy range considered. In order to comply with the phase convention of Ref. 15 we have to use the complex conjugate of Eq. (8).

For the ^{3}He+n channel, however, the immediate contribution b and the contribution due to coupling ia are of

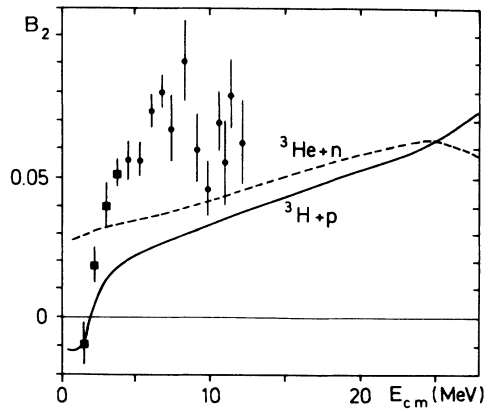

FIG. 5. Comparison of calculated B_2 coefficients, Eq. (9), with data Ref. 19 (full squares) and Ref. 20 (full circles).

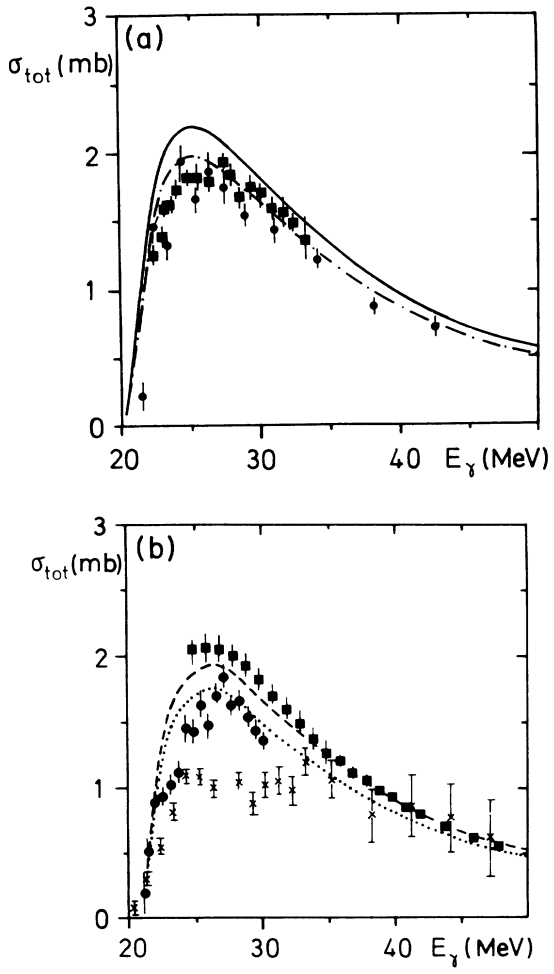

FIG. 6. (a) Comparison of calculated (γ,p) integrated photo breakup cross sections for 2.2% D-state admixture (full line) and 12% D-state admixture (dot-dashed line) with data Ref. 21 (full squares) and Ref. 22 (full circles). (b) Calculated (γ,n) integrated cross section for 2.2% D-state admixture (dashed line) and 12% D state (dotted line). The data are from Ref. 17 (full circles), Ref. 3 (pluses), and Ref. 23 (squares).

similar size, with $b > a$ at low energies and $b < a$ above 10 MeV. Therefore, the phase of the ^3He+n matrix element changes considerably because of the energy dependence of the imaginary part.

The different sign of the $E1$ matrix element is in accordance with the classical argument (see Fig. 3). This yields opposite signs for the A_1 and A_3 coefficients for the ^3H+p and ^3He+n capture reactions at low energies (see Fig. 2). Furthermore, the mixing of the corresponding channels gives rise to the different energy dependence of the A_1 and A_3 coefficients. The opposite signs of the A_1 and A_3 coefficients is perfectly found in the different angular distribution for the proton and neutron capture reactions (see Fig. 4). The differences originate from the Coulomb force without any isospin violating nucleon-nucleon force.

In analogy to the differential cross section we expand the vector analyzing power in terms of associated Legendre polynomials according to

$$\frac{d\sigma}{d\Omega}(\vartheta)A_y(\vartheta)=\sum_{n=1} B_n P_n(\cos\vartheta) \ . \tag{9}$$

It turns out that all coefficients B_n are small except for B_2. In Fig. 5 we compare the B_2 coefficient for ^3H+p and ^3He+n with data for the proton capture.[19,20] Unfortunately the large error bars do not allow any conclusion. All calculated coefficients agree in size and energy dependence with those of Ref. 5.

Originally, the possible isospin violation in electromagnetic transitions in ^4He was discussed for the total photo breakup cross sections. For the ratio R of $\sigma(\gamma,p)$ to $\sigma(\gamma,n)$ values up to 1.8 were reported,[4] whereas we find R below 1.1 in the energy range discussed.[4] In Fig. 6 we compare the calculated cross section with data for both reaction channels. In these figures we demonstrate the effect of the D-state admixture in the ^4He ground state (see Ref. 8). Whereas all previously shown results were calculated for 2.2% D-state admixture, we give here also the results for 12% D state. The only effect is a reduction by 10% as could be anticipated.

For $^4He(\gamma,p)^3H$ we reproduce the data within a few percent. For $^4He(\gamma,n)^3He$ however, we agree with part of the data[17,23] but disagree with others.[3] Thus our calculation yields results similar to those of the shell model calculation,[5] the main problem lies in the contradicting data, see the discussion on the data in Ref. 3.

In order to resolve the discrepancies of the data, Knoepfle *et al.*[24] performed $(e,e'x)$ reactions where all charged particles were detected simultaneously. Preliminary results[24] agree well with our calculations. Therefore, we conclude from our calculations that there are differences in the reactions $^3H(p,\gamma)^4He$ and $^3He(n,\gamma)^4He$ due to the Coulomb force and the different thresholds, however not due to any isospin violating nuclear force. The differences in the data call for new detailed experiments especially for the neutron branch which are planned at Karlsruhe.[25]

This work was partially supported by the German Federal Minister for Research and Technology (BMFT) under Contract No. 06 ER 771.

[1]V. König, W. Gruebler, R. A. Hardekopf, B. Jenny, R. Risler, H. R. Bürgi, P. A. Schmelzbach, and R. E. White, Nucl. Phys. **A331**, 1 (1979).

[2]F. C. Barker and A. K. Mann, Philos. Mag. **2**, 5 (1957).

[3]B. L. Berman, D. D. Faul, P. Meyer, and D. L. Olson, Phys. Rev. C **22**, 2273 (1980).

[4]J. R. Calarco, B. L. Berman, and T. W. Donnelly, Phys. Rev. C **27**, 1866 (1983).

[5]D. Halderson and R. J. Philpott, Nucl. Phys. **A359**, 365 (1981).
[6]F. C. Barker, Austr. J. Phys. **37**, 583 (1984).
[7]H. M. Hofmann, W. Zahn, and H. Stöwe, Nucl. Phys. **A357**, 139 (1981).
[8]B. Wachter, T. Mertelmeier, and H. M. Hofmann, Phys. Lett. B **200**, 246 (1988).
[9]J. L. Langenbrunner, G. Feldman, H. R. Weller, D. R. Tilley, B. Wachter, T. Mertelmeier, and H. M. Hofmann, Phys. Rev. C **38**, 565 (1988).
[10]T. Mertelmeier and H. M. Hofmann, Nucl. Phys. **A459**, 387 (1986).
[11]H. H. Hackenbroich, in *Proceedings of the International Symposium on the Present Status and Novel Developments in the Nuclear Many Body Problem, Rome, 1972,* edited by V. Calgero and C. Cioffi degli Atti (Editrico Compositori, Bologna, 1973).
[12]H. M. Hofmann, Lect. Notes Phys. **273**, 243 (1987).
[13]A. J. F. Siegert, Phys. Rev. **52**, 778 (1937).
[14]B. F. Gibson, Nucl. Phys. **A416**, 503c (1984).
[15]R. G. Seyler and H. R. Weller, Phys. Rev. C **20**, 453 (1979).
[16]R. C. McBroom, Ph.D. thesis, University of Florida, 1980 (unpublished).
[17]J. D. Irish, R. G. Johnson, B. L. Berman, B. J. Thomas, G. K. McNeill, and J. W. Jury, Can. J. Phys. **53**, 802 (1975).
[18]G. King III, Ph.D. thesis, Stanford, 1978 (unpublished).
[19]M. A. Kovash, Ph.D. thesis, Ohio State University, 1979 (unpublished).
[20]G. King, K. Wienhard, J. R. Calarco, and S. S. Hanna, Stanford University Report No. 7, 1976-77 (unpublished).
[21]W. E. Meyerhof, M. Suffert, and W. Feldman, Nucl. Phys. **A148**, 211 (1970).
[22]A. N. Gorbunov, Proc. of P. N. Lebedev Phys. Inst. **71**, 1 (1974).
[23]C. K. Malcom, D. V. Webb, Y. M. Shin, and D. M. Skopik, Phys. Lett. **47B**, 433 (1973).
[24]S. Khan, Th. Kihm, K. T. Knöpfle, H. J. Schulz, M. Spahn, J. Friedrich, N. Voegler, Ch. Schmitt, and V. H. Walther, Mâinz microtron annual report 1986-87, p. 128; private communication.
[25]H. O. Klages, private communication.